Hybrid-filtering-controlled pulse dynamics in mode-locked fiber lasers

Zengrun Wen,[1,2,3] Qinqin Zhang,[1,2,3] Xiulin Fan,[1,2,3] Kaile Wang,[4] Song Gao,[1,2,3] Weiming Wang,[1,2,3] Yangjian Cai,[1,2,3,*] and Yuanmei Gao[1,2,3,†]

[1]*Shandong Provincial Engineering and Technical Center of Light Manipulation and Shandong Provincial Key Laboratory of Optics and Photonic Devices, School of Physics and Electronics, Shandong Normal University, Jinan 250014, China*

[2]*Collaborative Innovation Center of Light Manipulation and Applications, Shandong Normal University, Jinan 250358, China*

[3]*Joint Research Center of Light Manipulation Science and Photonic Integrated Chip of East China Normal University and Shandong Normal University, East China Normal University, Shanghai 200241, China*

[4]*The State Key Laboratory of Integrated Service Networks, The School of Telecommunications Engineering, Xidian University, Xi'an 710071, China*

(Received 6 July 2023; revised 16 January 2024; accepted 26 February 2024; published 13 March 2024)

We numerically investigate the resembling pulse regimes in mode-locked fiber lasers through hybrid filtering implemented using super-Gaussian and sinusoidal spectral filters (SSFs). By modulating the saturation energy and filter bandwidth of the SSF, several stable regimes of resembling pulses including single, bounded, overlapped double resembling, and bounded triple resembling pulses can be produced. We explore the pulse characteristics of different single and bounded resembling pulses, such as the pulse intervals, chirps, optical spectra, and regime formation. During the transition between different mode-locked regimes, chaotic and pulsating pulses emerge, similar to the scenario of transitions induced by a single filter. Further study shows that synchronous and asynchronous power oscillations are produced in the pulse intensity and optical spectra when the laser operates at three typical pulsating states and one chaotic state. This paper reveals the effect of hybrid filtering on multipulse dynamics and proposes a method for modulating the mode-locking resembling pulses in fiber lasers.

DOI: 10.1103/PhysRevA.109.033513

I. INTRODUCTION

Mode-locked fiber lasers (MLFLs) are highly versatile and are used for generating various pulses or soliton sequences that are valuable in nonlinear scientific research and industrial applications [1]. As a type of nonlinear system with gain and loss, MLFLs not only facilitate the generation of stable solitons for specific applications but also support unstable soliton states including periodic pulsating solitons, breathers, soliton exploration, and chaotic regimes [2–5]. The pulse dynamics of MLFLs are highly dependent on the intracavity components such as saturable absorbers (SAs) and spectral filters or effects such as cavity dispersion and nonlinearity [6–8]. Researchers have developed various general strategies to obtain desired mode-locked pulses such as conventional solitons and dissipative solitons in anomalous and normal group-velocity dispersion laser configurations, respectively [9,10]. In addition to dispersion engineering, inverse saturable absorption effects support the formation of dissipative soliton resonances [11,12]. Spectral filters, also known as pulse shapers, play a crucial role in MLFLs with different configurations by facilitating dissipation and limiting optical spectrum broadening [13–16]. Over the past decade, the effects of filtering on mode-locked pulses have been investigated through numerical simulations and experimental studies. On one hand, the tuning of the spectrum bandwidth using band-pass filters (BPFs) or fiber Bragg gratings allows control over the transition of soliton regimes, leading to pulse splitting and soliton molecule formation and inducing intermediate pulsating solitons and intriguing abrupt nonlinear phenomena during the transition [17–21]. On the other hand, sinusoidal-type spectral filtering (SSF), implemented using the Lyot filter, multimode interference filter, or interferometer filter, facilitates the formation of laser pulses with multiple wavelengths or high repetition rates and induces diverse soliton regimes and state transitions [22–25].

In general, more than one filtering effect is observed in fiber lasers, as nearly each intracavity component has a bandwidth limit. If multiple filters are employed, their composite effect must be considered. Recent investigations have demonstrated that the utilization of multiple filters enhances the pulse manipulation ability, produces multiwavelength spectra, and suppresses the noise intensity [26–30]. For example, a composite filtering effect produced by a low-pass filter and comb filter can be used to switch the laser state from a single soliton to a soliton bunch [31,32]. Femtosecond and picosecond laser pulses can be switched by combining a nonlinear amplifier loop mirror filter and multimode interference filter [33]. The combination of a Lyot or Fabry-Pérot (F-P) filter in nonlinear polarization rotation (NPR) MLFLs is a way of controlling *h*-shaped pulses, soliton bunches, or dual-wavelength spectra [34–37]. *W*-shaped filters can be implemented by using three cascaded long-period gratings with enhanced tunability of the optical spectrum [38]. Additionally, composite filtering

*yangjiancai@sdnu.edu.cn
†gaoyuanmei@sdnu.edu.cn

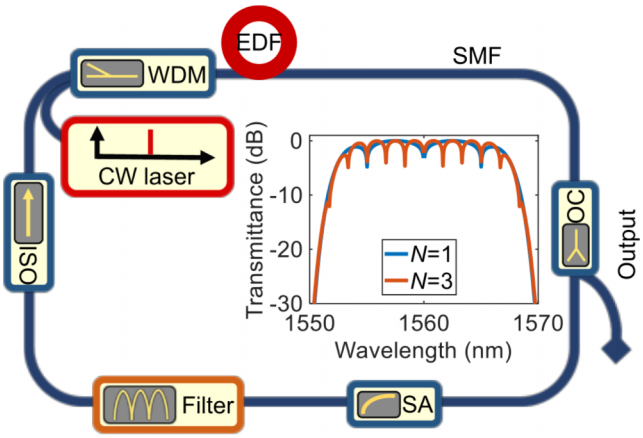

FIG. 1. Schematic model of the mode-locked ring fiber laser. Inset: Transmittance of the hybrid filter. WDM, wavelength division multiplexer; EDF, erbium-doped fiber laser; SMF, single-mode fiber; OC, optical coupler; ISO, isolator.

comprising NPR and F-P filters facilitates the generation of resembling pulses, which contain uniform or nonuniform modulated spikes across a pulse profile [39]. When the modulation depths of the spikes are large enough, the spikes are divided into discrete pulses. By incorporating two-stage Lyot filters in a fiber laser mode locked by NPR, the pulse intervals between solitons in the multipulse states can be tuned, manifesting the beneficial role of composite filtering in the generation and manipulation of resembling pulses [40]. The mode-locked resembling pulses can be numerically obtained using an SSF-based fiber laser with low saturation energy and short filtering period [41] through gain filtering; however, their transition dynamics have not yet been investigated.

In this paper, we numerically investigate the generation and transition of resembling pulse regimes in MLFLs via hybrid filtering. Hybrid filtering is achieved by combining a super-Gaussian filter and an SSF. A rigorous theoretical model that captures the unique effects of filtering is developed to simulate the responses of pulse dynamics as the saturation energy and period of the SSF are modulated. We extensively simulate the characteristics of different resembling pulse regimes, including pulse intensities, chirps, and optical spectra. The existence of pulsating and chaotic pulse regimes in the transition areas is also illustrated. This paper provides detailed insights into the generation and behavior of resembling pulse regimes through hybrid filtering in MLFLs.

II. THEORETICAL MODEL AND PRINCIPLE

The theoretical model of our laser uses a common ring cavity for all fiber mode-locked lasers, as depicted in Fig. 1. Four major components are connected by single-mode fibers (SMFs): a piece of erbium-doped fiber (EDF) pumped by a power-tunable continuous-wave laser diode through a wavelength division multiplexer to provide laser gain, an SA for achieving mode-locked pulses, a tunable hybrid filter used to shape the pulse, and an optical coupler to output 20% emission of laser pulses for measurement. The isolator guarantees unidirectional transmission of the laser pulse. According to the cavity configuration, a lumped scalar model considering all the components and fibers is utilized, in which the hybrid filter can be studied individually. In the numerical model, the pulse transmission in the fiber is governed by the scalar Ginzburg–Landau equation [42,43]

$$\frac{\partial \psi}{\partial z} = i\frac{\beta_2}{2}\frac{\partial^2 \psi}{\partial t^2} + i\gamma|\psi|^2\psi + g(z)\psi + \frac{g(z)}{\Omega_g^2}\frac{\partial^2 \psi}{\partial t^2}, \quad (1)$$

where ψ, β_2, γ, and Ω_g designate the pulse envelope, group-velocity dispersion, self-phase modulation coefficient, and gain bandwidth, respectively. The gain of the pumped EDF is described by $g(z)$. In the case of the passive fiber (SMF in the model), the value of $g(z)$ is zero. To characterize the saturable gain condition, $g(z)$ is expressed by $g(z) = g_0 \exp(-E_p/E_{\text{sat}})$, where g_0 is the small-signal gain coefficient and E_p depicts the pulse energy, which is a temporal integral of the pulse intensity. The saturation energy E_{sat} labels the change in pump power, whereas g_0 is invariant because of its small range of variation during pump modulation.

To achieve mode locking, an SA is modeled similar to the commonly used mode lockers such as saturable absorption materials [44], expressed as

$$T_{\text{SA}} = T_0 - \frac{\Delta T}{1 + |\psi|^2/P_{\text{sat}}}, \quad (2)$$

where T_0, ΔT, and P_{sat} denote the saturation transmission, modulation depth, and saturation power, respectively. After the SA, the hybrid filter is composed of a super-Gaussian filter and an SSF, the transmittance function of which is

$$T(\omega) = \frac{1}{2}\exp\left[-\left(\frac{\omega-\omega_0}{2\pi\Omega}\right)^{2n}\right]\left[1-\cos\frac{N(\omega-\omega_0)}{\Omega}\right], \quad (3)$$

where ω denotes the angular frequency. The central angular frequency ω_0 corresponds to the central wavelength of $\lambda_c =$ 1560 nm in this paper. The exponential and trigonometric terms represent the super-Gaussian filter ($n = 4$) and SSF, respectively [41,45]. We fixed the spectral width of the super-Gaussian filter by setting $\Omega = c\Delta\lambda/\lambda_c^2$, where $\Delta\lambda = 5$ nm. The value of N characterizes the period of SSF. Two examples of transmittance of hybrid filtering are depicted in the inset of Fig. 1. The variation in N alters the modulation frequency across the super-Gaussian envelope. It should be noted that the filtering described by Eq. (3) can be implemented by connecting a comb filter (such as a Lyot filter [46], SMF-graded-index multi-mode fiber-SMF structure [47], F-P interferometer [23], or special pulse shaper [48]) and a BPF in series.

In the theoretical model, we employ Eq. (1) when the pulse is transmitted in EDF or SMF, whereas the corresponding transmittance function is used for the cavity components. Equation (1) is numerically solved by the symmetric split-step Fourier-transform method [49]. The simulation starts with a weak pulse in the EDF instead of white noise of spontaneous radiation, for quick convergence. The stable pulse regimes are universally obtained within 1000 round trips (RTs). Therefore, it is valid to terminate the simulation after 2000 RTs.

The simulation parameters are as follows: (i) $\beta_2 =$ 29.53 ps^2/km, $\gamma = 3.0$ W^{-1} km^{-1}, $g_0 = 3$ m^{-1}, and $\Omega_g =$ 30 nm for the EDF; (ii) $\beta_2 = -23.0$ ps^2/km and $\gamma =$ 1.3 W^{-1} km^{-1} for the SMF; and (iii) $T_0 = 0.6$, $\Delta T = 0.2$, and

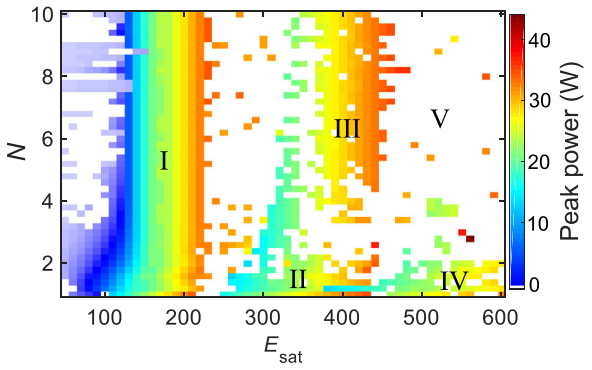

FIG. 2. Pulse peak power of steady mode-locked regimes vs saturation energy E_{sat} and N. Five pulse regimes are marked: I, single resembling pulse; II, bounded double resembling pulses; III, overlapped double resembling pulses; IV, triple resembling pulses; V, unstable mode-locked states.

$P_{sat} = 100$ W for the SA. The lengths of the EDF and SMF are 0.6 and 5 m, respectively, corresponding to a net dispersion of -0.097 ps^2. In the simulation process, we tune the saturation energy E_{sat} and N within the ranges of 50–600 pJ and 1–10, respectively.

III. RESULTS AND DISCUSSION

A. State transition map of resembling pulses

To systematically investigate the effects of hybrid filtering on mode-locked resembling pulses, we conducted simulations over the modulation of saturation energy E_{sat} and N with gradients of 10 pJ and 0.2, respectively. At the end of each simulation, the pulse peak power based on the final RT was extracted, the collection of which is shown in Fig. 2. To determine the operating state of the laser, we calculated the normalized rms of the pulses over the last 100 RTs. If the rms value was less than 1, the laser was assumed to operate in a chaotic or pulsating state, which corresponded to the white area (V) in Fig. 2. According to the principle of color change and pulse characteristics [19], the map was divided into four regions marked I–IV, which were labeled as a single pulse state (I), bounded double resembling pulse state (II), overlapped resembling pulse state (III), and bounded triple resembling pulse state (IV). Between the different regions, chaotic or pulsating regimes were observed, similar to those observed during the transition of mode-locked multipulsing [50,51]. The transition between regions II and III was induced by the period of the SSF, whereas the other transitions between stable regimes were a result of changes in the saturation energy E_{sat}. This suggests that the combination of E_{sat} and super-Gaussian filtering leads to the splitting of resembling pulses. In the stable regions, the pulse peak power gradually increased with increasing E_{sat}. Simultaneously, a decrease in the period of SSF reduced the peak power within the range of $N < 3.2$. However, for $3.2 < N < 10$, the peak power remained nearly constant with respect to N. Consequently, the pulse splitting transition occurred first for small values of N, resulting in the generation of stable bounded triple pulses with $N < 2$. If the period of the SSF was small ($N > 4.2$), the bounded triple resembling pulses no longer existed. Region III was larger than region II, indicating that the overlapped double resembling pulses had better robustness than the bounded double resembling pulses, against modulation of the filter. Furthermore, the minimum peak power area was observed in the range of $50 < E_{sat} < 100$ pJ and $7.8 < N < 9$, where the SSF dominated the pulse shape and formed soliton macromolecules. Conversely, the maximum peak power was distributed at the right edges of the stable areas. When the saturation energy was increased further, the pulse could split. The overlapped resembling pulses in region III were formed from bounded double resembling pulses, which required a smaller SSF period and larger saturation energy.

B. Single resembling pulses

The pulse characteristics including pulse intensities, spectra, and formation processes were concretely investigated for the five regions of mode locking. First, we focused on the stable single resembling pulses, corresponding to region I in Fig. 2. Three typical results are illustrated in Fig. 3. For a low saturation energy E_{sat} and small N value, hybrid filtering supported a single soliton pulse, as shown in Figs. 3(a1)–3(a4). In this case, the filtering gain was narrow. Thus, two main filtering peaks existed to form dual walk-off pulses with dual wavelengths when the laser was started. The pulse walk-off originated from the discrepancy of peaks between gain and filtering [52]. After cycling for 600 RTs, one of the dual pulses was annihilated and the other pulse was gradually reshaped to a steady pulse. Simultaneously, only the left peak of the spectrum was preserved, as depicted in Fig. 3(a2). The stable pulse intensity and spectrum are displayed in Figs. 3(a3) and 3(a4), respectively. The absence of a Kelly sideband on the spectrum and the linear up-frequency chirp indicate that the pulse shaping is dominated by filtering [41]. Next, by increasing the saturation energy or reducing the period of the SSF, a single resembling pulse was formed quickly without walk-off. This pulse contained seven solitons with uniform spacing, symmetrically distributed about zero time, as shown in Figs. 3(b1)–3(b4). The chirp exhibited inverse symmetry about the central time. Symmetric spikes were observed on the spectrum, which were consistent with the filtering peaks. Furthermore, when the saturation energy was further increased to 170 pJ, a symmetric resembling pulse about zero time was formed during the initial 1000 RTs, which then underwent changes in soliton distribution. The first soliton on the left and central solitons reduced, while the first soliton on the right gradually grew to match the profile of the central soliton, as depicted in Fig. 3(c1). Figure 3(c3) intuitively shows the difference between the resembling states of 1000 and 2000 RTs. The newly generated one contained three soliton pairs symmetrically distributed around the center of the two peaks. The positions of the spikes in the spectrum remained unchanged, but the modulation depth increased. This variation in resembling pulses arose from the stronger interplay between solitons owing to the larger saturation energy. As a result, energy exchange occurred between adjacent solitons, leading to the formation of identical soliton pairs, similar to the process of soliton molecules [53]. According to the simulation results, there are three single pulse states in region I of Fig. 2,

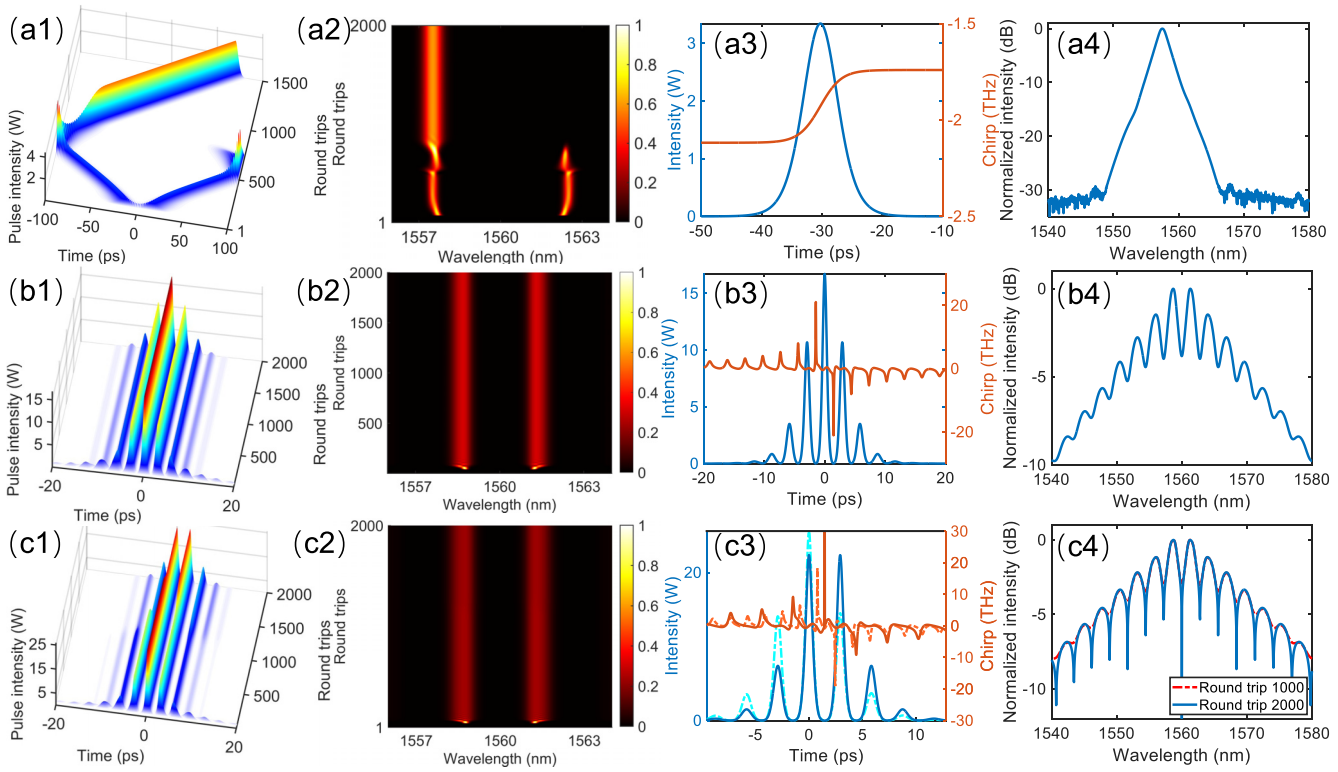

FIG. 3. Characteristics of single pulse states. (a1, a2) Spatial-temporal evolution of pulse intensity and spectral intensity of the single pulse state with $N = 1$ and $E_{sat} = 80$ pJ. (a3) Pulse intensity profile and chirp. (a4) Optical spectrum of the steady single pulse state. Panels (b1)–(b4) and (c1)–(c4) are the same as panels (a1)–(a4) with $E_{sat} = 140$ pJ, $N = 1.8$ and $E_{sat} = 170$ pJ, $N = 1.8$, respectively.

manifesting the diverse pulse-shaping capabilities of hybrid filtering.

To illustrate the effect of SSF period on the single resembling pulse, we performed a simulation on the stable output pulse with a fixed saturation energy of 180 pJ while modulating the value of N. The results for N of 1, 3, 5, and 10 are presented in Fig. 4. A shorter SSF period increases the number of spikes on the optical spectrum. Owing to the Fourier-transform relation between the temporal pulse and spectrum, the temporal interval between solitons increases. Consequently, the resembling pulses exhibit broadening. Additionally, as N increases, the difference in peak amplitudes between solitons increases, which can be attributed to the finite gain bandwidth. In the process, no evident Kelly sideband is observed because of the narrow super-Gaussian filtering. The results demonstrate that the period of SSF plays a crucial role in manipulating the resembling pulses.

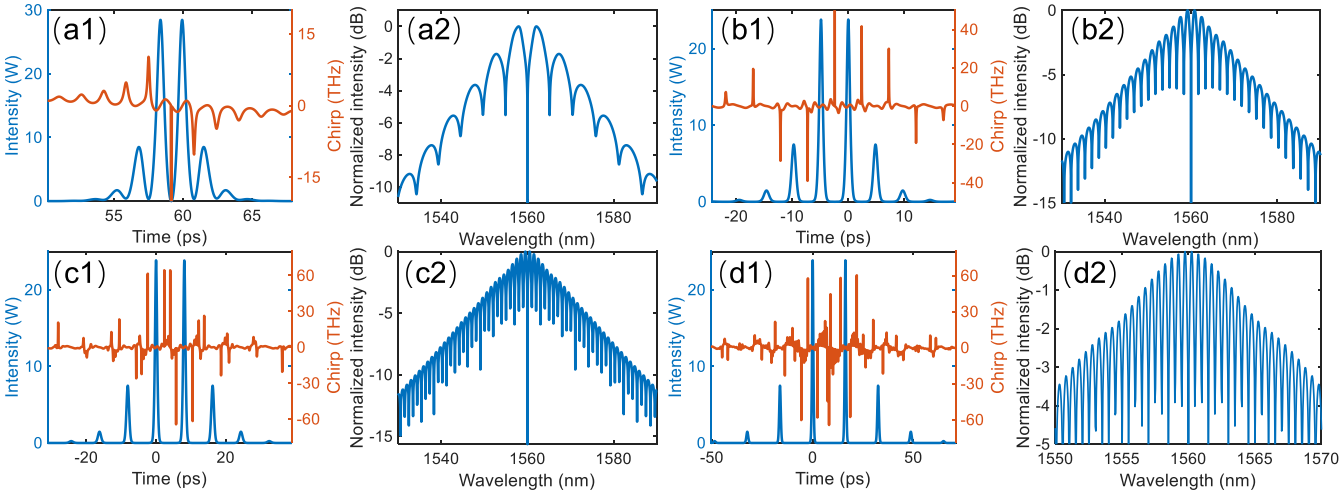

FIG. 4. Pulse intensities, chirps, and optical spectra with different N of (a1, a2) 1, (b1, b2) 3, (c1, c2) 5, and (d1, d2) 10, when E_{sat} is fixed at 180 pJ.

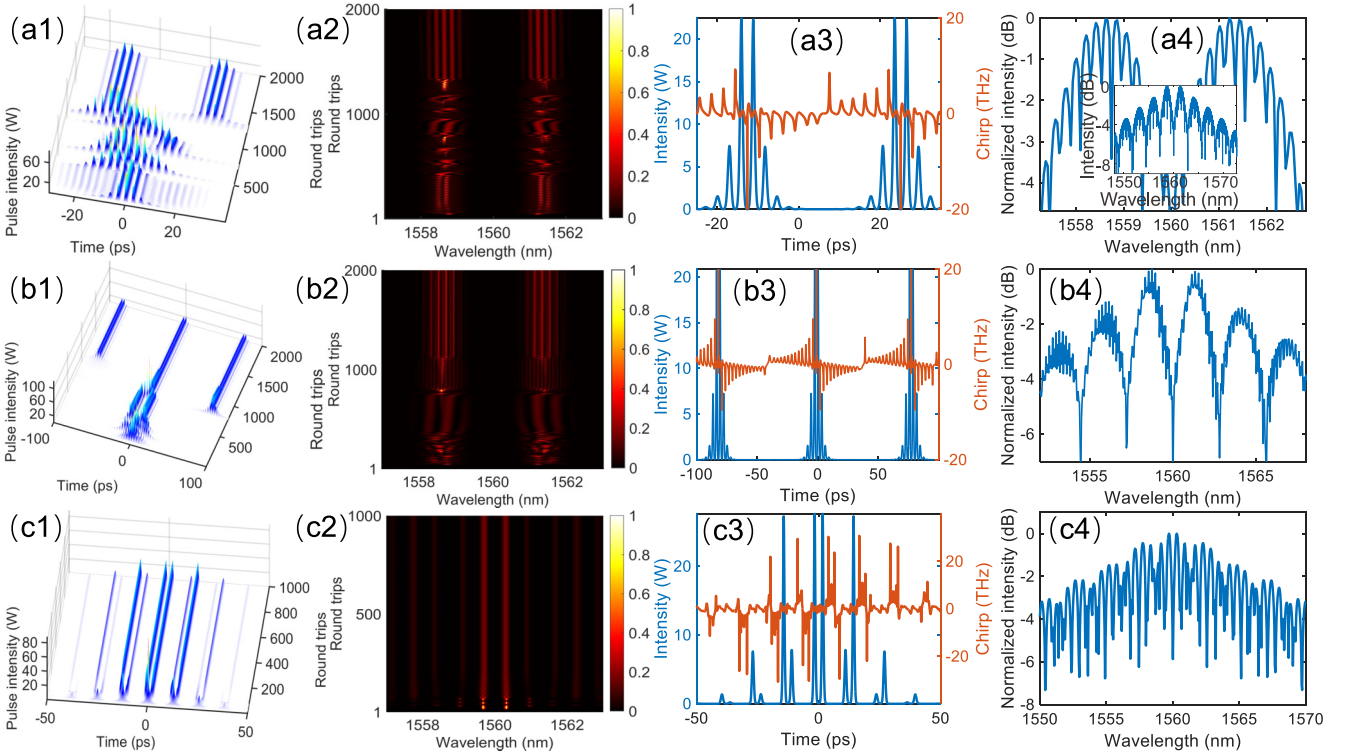

FIG. 5. Bound states of resembling pulses. (a1) Formation process of double resembling pulses with $E_{\mathrm{sat}} = 340$ pJ and $N = 1.8$. (a2) Optical spectrum evolution. (a3) Steady pulse intensity and chirp. (a4) Optical spectrum. (b1–b4, c1–c4) Triple and overlapped resembling pulses with $E_{\mathrm{sat}} = 490$ pJ, $N = 1.8$ and $E_{\mathrm{sat}} = 390$ pJ, $N = 7.8$, respectively.

C. Bound states of resembling pulses

As the saturation energy increases, the single resembling pulse in the laser undergoes splitting, eventually forming stable bounded resembling pulses or overlapped resembling pulses, depending on the hybrid filtering and E_{sat}. These mode-locked states correspond to regions II, III, and IV in Fig. 2. The pulse characteristics of these states are illustrated in Fig. 5. As shown in Fig. 5(a1), a single resembling pulse is initially formed in the laser, which is broadened and shifted during 400–1300 RTs. Finally, the dispersion wave background converges to form two stable resembling pulses. The optical spectrum shown in Fig. 5(b) exhibits two main spectral peaks symmetrically distributed around 1560 nm after undergoing a transient process. Figure 5(a3) depicts the stable states of the two resembling pulses, which possess identical pulse profiles and frequency chirps. The optical spectrum in Fig. 5(a4) manifests intensity modulation on the spectral envelopes, with a modulation frequency corresponding to the temporal interval between the two resembling pulses. The pulse characteristics of the bound-state soliton indicate that the two resembling pulses are in a bound state [54]. By setting $E_{\mathrm{sat}} = 490$ pJ and $N = 1.8$, the bounded triple resembling pulse state is obtained, the pulse characteristics of which are displayed in Figs. 5(b1)–5(b4). In this configuration, the initially generated single resembling pulse splits into two bounded resembling pulses, which then converge to form a high intensity peak. However, the pulse with high intensity is unstable in the laser and splits again, resulting in two resembling pulses with a larger interval. Eventually, bounded triple resembling pulses are formed. Figure 5(b3) shows that the intensity profile and chirp of the three resembling pulses are completely consistent, while the intervals between the pulses are different. Similar to the previous case, intensity modulation occurs in the optical spectrum, as shown in Fig. 5(b4). Overlapped resembling pulses are generated in region III of Fig. 2; a typical result is shown in Figs. 5(c1)–5(c4). The temporal evolution shows that this regime is formed more rapidly than the one involving bounded resembling pulses. As shown in Fig. 5(c3), the two resembling pulses overlap, with the two solitons in the center bounded tightly. The shape of the optical spectrum of this regime is similar to that of the multipulse bound state [55].

The transition from bounded double resembling pulse to overlapped resembling pulse states can be achieved by tuning the period of the SSF. In Fig. 6, five pulse intensities are displayed to illustrate the variations in the pulse characteristics of the two mode-locked regimes. When the period of the SSF is large, the chirps of the two bounded resembling pulses are opposite [Fig. 6(a)]. By reducing the filter period, the chirps of the two pulses become identical and their intervals are shortened, as depicted in Fig. 6(b). As the filter period is reduced further, the pulse interval continues to shrink with chirp inversion, finally leading to overlapped resembling pulses, as shown in Figs. 6(c) and 6(d). In the overlapped resembling state, as seen in the comparison presented in Figs 6(e), the soliton intervals are enlarged with the reduction of the SSF period, except for the two solitons in the center. The autocorrelation traces of the two mode-locked regimes are shown in

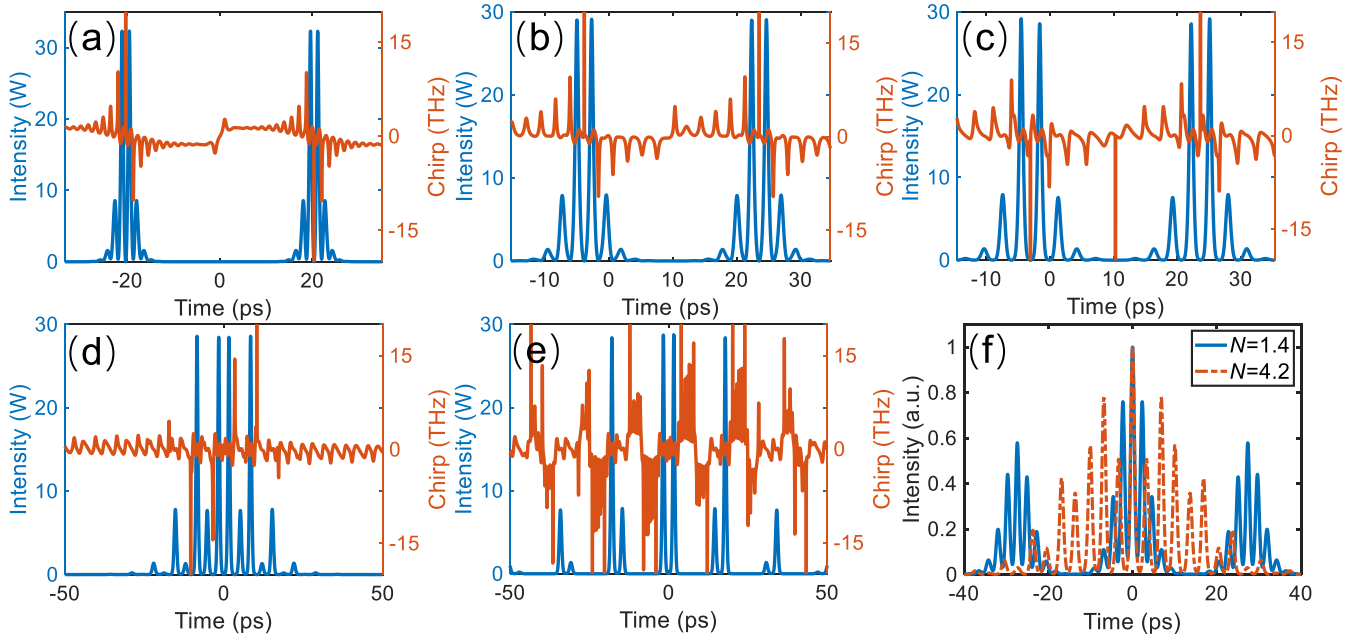

FIG. 6. Pulse intensities of bounded resembling pulses for different N of (a) 1, (b) 1.2, (c) 1.4, (d) 1.8, and (e) 4.2. (f) Autocorrelation traces for $N = 1.4$ and 4.2. All results correspond to $E_{\text{sat}} = 400$ pJ.

Fig. 6(f). In the case of bounded double resembling pulses, three separate peaks with intensity modulation manifest so that the two resembling pulses are in the bounded state. For the overlapped resembling pulse state, there is only one main peak with intensity modulation, indicating that the solitons in this state can be viewed as one integrated pulse.

D. Pulsing and chaotic regimes

As discussed in Sec. III A, pulsating and chaotic resembling pulses are formed during the transition between the stable mode-locked regimes. Similar to the pulsating solitons in the MLFLs, these pulsating resembling pulses exhibit periodic changes in the pulse peak intensity, with respect to cavity RTs, as shown in Fig. 7. For a single resembling pulse in Figs. 7(a1) and 7(a2), the soliton peaks within the pulse oscillate synchronously with a period of 17 RTs. In the optical spectrum, the wavelengths of the two main peaks vary periodically and symmetrically within a small range, accompanied by peak oscillations. When the saturation energy and value of N are set to 390 pJ and 2.8, respectively, a pulsating bounded double resembling pulse is obtained. The pulse evolution and spectrum variations are displayed in Figs. 7(b1) and 7(b2). In this case, the solitons in each of the two resembling pulses

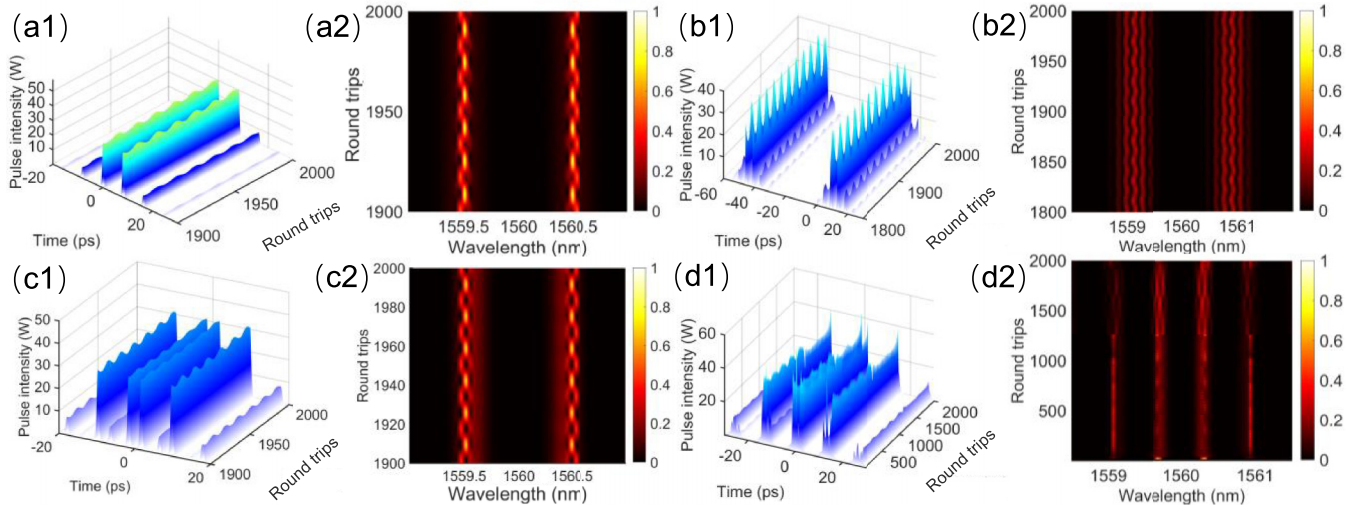

FIG. 7. Pulsating and chaotic resembling pulse states corresponding to the white area V in Fig. 2. (a1, a2) Pulse intensity and spectrum evolution of the single resembling pulse with $E_{\text{sat}} = 300$ pJ and $N = 5$. (b1, b2) Pulse intensity and spectrum of bounded double resembling pulses with $E_{\text{sat}} = 390$ pJ and $N = 2.8$. (c1, c2) Transmission of pulse intensity and spectrum of overlapped double resembling pulses with $E_{\text{sat}} = 500$ pJ and $N = 5$. (d1, d2) Pulse intensity and spectrum of the chaotic state with $E_{\text{sat}} = 550$ pJ and $N = 8$.

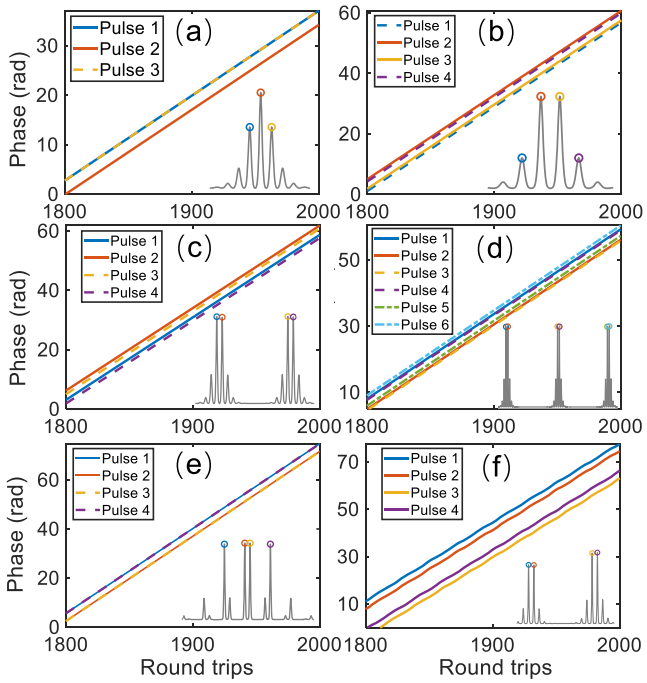

FIG. 8. Phase evolution as a function of round trip for different pulse regimes with (a) $E_{\text{sat}} = 140$ pJ, $N = 1.8$; (b) $E_{\text{sat}} = 170$ pJ, $N = 1.8$; (c) $E_{\text{sat}} = 340$ pJ, $N = 1.8$; (d) $E_{\text{sat}} = 490$ pJ, $N = 1.8$; (e) $E_{\text{sat}} = 390$ pJ, $N = 7.8$; and (f) $E_{\text{sat}} = 550$ pJ, $N = 8$.

oscillate synchronously, but asynchronous oscillations occur between the two resembling pulses. The peaks of the two wavelengths vibrate transversely, and the patterns are asymmetric about the wavelength of 1560 nm. Figures 7(c1) and 7(c2) depict the pulsating states of the overlapped resembling pulse. The dynamic behaviors are similar to that of a pulsating single resembling pulse. In the chaotic state, the resembling pulse cannot reach a steady state as it cycles in the laser. An example is shown in Figs. 7(d1) and 7(d2); all solitons oscillate synchronously, but there is no stable pattern over the whole RT. Correspondingly, the spectrum, limited by filtering, is also unstable and is accompanied by the energy exchange between different wavelengths.

IV. CONCLUSIONS

The resembling pulse dynamics in MLFLs operating in anomalous dispersion regimes were numerically investigated. We employed a lumped numerical model of mode locking that considered all the intracavity components individually to simulate the mode-locked states. By scanning two parameters, namely, the saturation energy E_{sat} and N, five distinct regions were identified: the single pulse state, bounded double resembling pulse state, overlapped resembling pulse state, bounded triple resembling pulse state, and unstable state. In the single pulse state, transitions occurred from a linear chirped pulse to two types of resembling pulse by modulating the saturation energy and period of the SSF. Reducing the SSF period increased the spikes in the optical spectrum envelope, thereby broadening the resembling pulse. For the multiresembling state, typical characteristics including pulse intensity, chirp, and spectrum of bounded double and triple resembling pulses were depicted. The transition from bounded double resembling pulses to overlapped resembling pulses was achieved by tuning the SSF period. Three pulsating resembling regimes and one chaotic state were analyzed. The developed numerical model can be easily migrated to other types of MLFLs with dispersion management for demonstrating the hybrid-filtering effect in various laser configurations.

ACKNOWLEDGMENTS

We acknowledge the support of the National Natural Science Foundation of China (Grants No. 12104272, No. 91950104, No. 12147155, and No. 12104265) and the Taishan Scholar Project of the Shandong Province (Grant No. tsqnz20221132).

APPENDIX: PHASE EVOLUTION OF DIFFERENT PULSE REGIMES

For a bound soliton or soliton molecules, a certain phase relation exists between the solitons. If the phase difference between the solitons in the bound states is 0, π, or $\pi/2$, the solitons can be steady in the MLFLs [56]. The phase changes of the pulses in different resembling pulse regimes are extracted and displayed in Fig. 8. The different phases corresponding to the pulses are marked by colored circles in the inset of each figure. When the laser operates in the stable state, the phases increase linearly against RT, indicating certain phase relations between different pulses. Figure 8(a) shows that pulse 1 has a phase identical to that of pulse 3, while there is a phase difference of 1.1π between both pulses and the central pulse (pulse 2). For the single resembling pulse obtained by raising $E_{\text{sat}} = 170$ pJ, as illustrated in Fig. 8(b), the phase difference between the two central pulses (pulse 2 and pulse 3) is π. The same case occurs between pulse 1 and pulse 4. Figures 8(c) and 8(d) show the phase changes of the double and triple resembling pulses. The phase difference between the adjacent central pulses in every resembling pulse is π. For the overlapped resembling pulse, identical phases exist between pulse 1 and pulse 4 and between pulse 2 and pulse 3. When the laser operates in periodically pulsating resembling pulse states, the phases of the four pulses vary synchronously. The phase difference of π between pulse 1 and pulse 2 and between pulse 3 and pulse 4 remains invariant. Therefore, we conclude that the two resembling pulses in the double resembling pulse regime are bounded.

[1] P. Grelu and N. Akhmediev, Dissipative solitons for mode-locked lasers, Nat. Photonics **6**, 84 (2012).

[2] X. Wang, J. He, B. Mao, H. Guo, Z. Wang, Y. Yue, and Y.-g. Liu, Real-time observation of dissociation dynamics within a pulsating soliton molecule, Opt. Express **27**, 28214 (2019).

[3] R.-R. Wang, W.-B. Bo, H.-B. Han, C.-Q. Dai, and Y.-Y. Wang, Vector pulsating solitons and soliton molecules under

higher-order effects in passively mode-locked fiber lasers, Chaos, Solitons Fractals **171**, 113438 (2023).
[4] G. Xu, A. Gelash, A. Chabchoub, V. Zakharov, and B. Kibler, Breather wave molecules, Phys. Rev. Lett. **122**, 084101 (2019).
[5] M. Liu, T.-J. Li, A.-P. Luo, W.-C. Xu, and Z.-C. Luo, "Periodic" soliton explosions in a dual-wavelength mode-locked Yb-doped fiber laser, Photonics Res. **8**, 246 (2020).
[6] C. Ouyang, L. Chai, H. Zhao, M. Hu, Y. Song, Y. Li, and C. Wang, Pulse-shaping dynamics controlled by four structural parameters in an all-normal-dispersion mode-locked fiber laser, J. Opt. Soc. Am. B **26**, 1875 (2009).
[7] B. G. Bale, J. N. Kutz, A. Chong, W. H. Renninger, and F. W. Wise, Spectral filtering for high-energy mode-locking in normal dispersion fiber lasers, J. Opt. Soc. Am. B **25**, 1763 (2008).
[8] H. Kotb, M. A. Abdelalim, and H. Anis, Effect of narrow spectral filter position on the characteristics of active similariton mode-locked femtosecond fiber laser, Opt. Express **23**, 29660 (2015).
[9] L. M. Zhao, D. Y. Tang, H. Zhang, X. Wu, and N. Xiang, Soliton trapping in fiber lasers, Opt. Express **16**, 9528 (2008).
[10] R. I. Woodward, Dispersion engineering of mode-locked fibre lasers, J. Opt. **20**, 033002 (2018).
[11] D. Li, D. Tang, L. Zhao, and D. Shen, Mechanism of dissipative-soliton-resonance generation in passively mode-locked all-normal-dispersion fiber lasers, J. Lightwave Technol. **33**, 3781 (2015).
[12] X. Li, X. Huang, E. Chen, Y. Zhou, and Y. Han, Dissipative-soliton-resonance and evolution in an all-normal dispersion Er-doped fiber laser, Opt. Laser Technol. **156**, 108592 (2022).
[13] J. B. Schroeder, S. Coen, T. Sylvestre, and B. J. Eggleton, Dark and bright pulse passive mode-locked laser with in-cavity pulse-shaper, Opt. Express **18**, 22715 (2010).
[14] S. Boscolo, C. Finot, H. Karakuzu, and P. Petropoulos, Pulse shaping in mode-locked fiber lasers by in-cavity spectral filter, Opt. Lett. **39**, 438 (2014).
[15] S. Boscolo, C. Finot, and S. K. Turitsyn, Bandwidth programmable optical Nyquist pulse generation in passively mode-locked fiber laser, IEEE Photonics J. **7**, 1 (2015).
[16] R. I. Woodward, E. J. R. Kelleher, T. H. Runcorn, S. Loranger, D. Popa, V. J. Wittwer, A. C. Ferrari, S. V. Popov, R. Kashyap, and J. R. Taylor, Fiber grating compression of giant-chirped nanosecond pulses from an ultra-long nanotube mode-locked fiber laser, Opt. Lett. **40**, 387 (2015).
[17] M. Alsaleh, T. Uthayakumar, E. Tchomgo Felenou, P. Tchofo Dinda, P. Grelu, and K. Porsezian, Pulse breaking through spectral filtering in dispersion-managed fiber lasers, J. Opt. Soc. Am. B **35**, 276 (2018).
[18] Z. Wang, L. Zhan, X. Fang, and H. Luo, Spectral filtering effect on mode-locking regimes transition: similariton-dissipative soliton fiber laser, J. Opt. Soc. Am. B **34**, 2325 (2017).
[19] Z. Wen, B. Lu, X. Qi, C. Zhang, K. Wang, H. Chen, and J. Bai, Effects of spectral filtering on pulse dynamics in a mode-locked fiber laser with a bandwidth tunable filter, J. Opt. Soc. Am. B **36**, 952 (2019).
[20] B. Dutta Gupta, S. Das Chowdhury, D. Dhirhe, and M. Pal, Intermittent events due to spectral filtering induced multi-pulsing instability in a mode-locked fiber laser, J. Opt. Soc. Am. B **37**, 2278 (2020).
[21] P. T. Dinda, A. Malfondet, P. Grelu, G. Millot, and A. Kamagate, Strategies for accessing the multipulse regime of mode-locked fiber lasers, Phys. Rev. A **107**, 033513 (2023).
[22] A. Khanolkar and A. Chong, Multipulsing states management in all-normal dispersion fiber laser with a fiber-based spectral filter, Opt. Lett. **45**, 6374 (2020).
[23] X.-M. Tan, H.-J. Chen, H. Cui, Y.-K. Lv, G.-K. Zhao, Z.-C. Luo, A.-P. Luo, and W.-C. Xu, Tunable and switchable dual-waveband ultrafast fiber laser with 100 GHz repetition-rate, Opt. Express **25**, 16291 (2017).
[24] Q. Gao, Y. Du, Z. He, D. Mao, and J. Zhao, Narrowband mode-locked fiber laser via spectral-domain intermodal interference, J. Lightwave Technol. **39**, 6276 (2021).
[25] Z. Wen, W. Wang, S. Gao, K. Wang, Y. Cai, and Y. Gao, Soliton macromolecule dynamics in fiber lasers with sinusoidal filtered nonlinear optical loop mirror, Phys. Rev. A **106**, 023522 (2022).
[26] Z. Zhang, L. Zhan, K. Xu, J. Wu, Y. Xia, and J. Lin, Multi-wavelength fiber laser with fine adjustment, based on nonlinear polarization rotation and birefringence fiber filter, Opt. Lett. **33**, 324 (2008).
[27] S. Wang, P. Lu, S. Zhao, D. Liu, W. Yang, and J. Zhang, 2-μm switchable dual-wavelength fiber laser with cascaded filter structure based on dual-channel Mach–Zehnder interferometer and spatial mode beating effect, Appl. Phys. B **117**, 563 (2014).
[28] D. Kim, S. Zhang, D. Kwon, R. Liao, Y. Cui, Z. Zhang, Y. Song, and J. Kim, Intensity noise suppression in mode-locked fiber lasers by double optical bandpass filtering, Opt. Lett. **42**, 4095 (2017).
[29] Y. Chang, L. Pei, T. Ning, and J. Zheng, Switchable multi-wavelength fiber laser based on hybrid structure optical fiber filter, Opt. Laser Technol. **124**, 105985 (2020).
[30] W. He, H. Yuan, X. Lou, L. Zhu, and M. Dong, Multi-wavelength switchable erbium-doped fiber laser based on a hybrid filter incorporating a bi-tapered Mach–Zehnder interferometer and Sagnac loop, Phys. Scr. **94**, 125502 (2019).
[31] C. Bao, X. Xiao, and C. Yang, Soliton rains in a normal dispersion fiber laser with dual-filter, Opt. Lett. **38**, 1875 (2013).
[32] Y. Zhou, W. Lin, H. Cheng, W. Wang, T. Qiao, Q. Qian, S. Xu, and Z. Yang, Composite filtering effect in a SESAM mode-locked fiber laser with a 3.2-GHz fundamental repetition rate: switchable states from single soliton to pulse bunch, Opt. Express **26**, 10842 (2018).
[33] J.-W. Wu, G.-X. Liu, Y.-X. Gao, X.-B. Lin, H. Cui, Z.-C. Luo, W.-C. Xu, M. E. Likhachev, S. S. Aleshkina, V. M. Mashinsky, M. V. Yashkov, and A.-P. Luo, Switchable femtosecond and picosecond spatiotemporal mode-locked fiber laser based on NALM and multimode interference filtering effects, Opt. Laser Technol. **155**, 108414 (2022).
[34] L. Gu, Z. Liu, Y. Shu, Z. Cui, K. Zhou, J. Li, A. Luo, and W. Chen, Artificial manipulation of h-shaped pulse generation by synthetizing composite filtering effects, Opt. Laser Technol. **157**, 108659 (2023).
[35] J.-M. Jiang, X.-J. Chen, Y.-X. Gao, M. Liu, Z.-A. Bai, A.-P. Luo, W.-C. Xu, and Z.-C. Luo, Bidirectional ultrahigh-repetition-rate ultrafast fiber laser, Opt. Laser Technol. **142**, 107196 (2021).
[36] L. Gu, Z. Cui, Y. Shu, M. Li, J. Li, A. Luo, and W. Chen, Switchable generation of dual-wavelength homogeneous and

heterogeneous pulse patterns in a double-cavity fiber laser, Infrared Phys. Technol. **121**, 104042 (2022).

[37] Q. Zhao, L. Pei, J. Zheng, M. Tang, Y. Xie, J. Li, and T. Ning, Tunable and interval-adjustable multi-wavelength erbium-doped fiber laser based on cascaded filters with the assistance of NPR, Opt. Laser Technol. **131**, 106387 (2020).

[38] J. Wang, A. Ping Zhang, Y. H. Shen, H.-y. Tam, and P. K. A. Wai, Widely tunable mode-locked fiber laser using carbon nanotube and LPG W-shaped filter, Opt. Lett. **40**, 4329 (2015).

[39] W. Chen, W. Lin, T. Qiao, and Z. Yang, Additive mode-locked resembling pulses in a Tm-doped fiber laser with a hybrid cavity configuration, Opt. Express **23**, 28012 (2015).

[40] Z. Liu, L. Gu, J. Li, and W. Chen, Manipulation of tunable soliton molecule generation in a fiber laser, Infrared Phys. Technol. **130**, 104618 (2023).

[41] K. Zhao, X. Xiao, and C. Yang, Sinusoidal spectral filtering-based soliton dynamics in mode-locked fiber lasers, IEEE J. Sel. Top. Quantum Electron. **28**, 1 (2022).

[42] J. Lee, S. Kwon, and J. H. Lee, Numerical investigation of the impact of the saturable absorber recovery time on the mode-locking performance of fiber lasers, J. Lightwave Technol. **38**, 4124 (2020).

[43] S. Yang, Z. Zhu, Y. Qi, L. Jin, L. Li, and X. Lin, Internal motion within pulsating pure-quartic soliton molecules in a fiber laser, Chaos, Solitons Fractals **172**, 113544 (2023).

[44] B. Wang, H. Han, L. Yu, Y. Wang, and C. Dai, Generation and dynamics of soliton and soliton molecules from a VSe_2 /GO-based fiber laser, Nanophotonics **11**, 129 (2022).

[45] R. Xu, F. Xu, Y. Song, L. Duan, Y. Song, S. Tan, and Z. Liu, Impact of spectral filtering on pulse breaking-up and noise-like pulse generation in all-normal dispersion fiber lasers, Opt. Express **28**, 21348 (2020).

[46] D. Han, L. Mei, Z. Hui, A.-H. Soliman, K. Ren, Y. Zheng, T. Li, and J. Gong, Flexible wavelength-, pulse-controlled mode-locked all-fiber laser based on a fiber Lyot filter, Opt. Express **30**, 41271 (2022).

[47] G. Chen, W. Li, G. Wang, W. Zhang, C. Zeng, and W. Zhao, Generation of coexisting high-energy pulses in a mode-locked all-fiber laser with a nonlinear multimodal interference technique, Photonics Res. **7**, 187 (2019).

[48] J. P. Lourdesamy, A. F. J. Runge, T. J. Alexander, D. D. Hudson, A. Blanco-Redondo, and C. M. de Sterke, Spectrally periodic pulses for enhancement of optical nonlinear effects, Nat. Phys. **18**, 59 (2022).

[49] G. P. Agrawal, *Nonlinear Fiber Optics*, 5th ed. (Academic, New York, 2013).

[50] B. G. Bale, K. Kieu, J. N. Kutz, and F. Wise, Transition dynamics for multi-pulsing in mode-locked lasers, Opt. Express **17**, 23137 (2009).

[51] X. Zhang, F. Li, K. Nakkeeran, J. Yuan, Z. Kang, J. N. Kutz, and P. K. A. Wai, Impact of spectral filtering on multipulsing instability in mode-locked fiber lasers, IEEE J. Sel. Top. Quantum Electron. **24**, 1 (2018).

[52] Z. Wen, K. Wang, H. Chen, B. Lu, and J. Bai, Stable-, period-N- and multiple-soliton regimes in a mode-locked fiber laser with inconsistently filtered central wavelengths, Opt. Express **28**, 28033 (2020).

[53] Z. Q. Wang, K. Nithyanandan, A. Coillet, P. Tchofo-Dinda, and Ph. Grelu, Optical soliton molecular complexes in a passively mode-locked fibre laser, Nat. Commun. **10**, 830 (2019).

[54] Y. Zhou, J. Shi, Y.-X. Ren, and K. K. Y. Wong, Reconfigurable dynamics of optical soliton molecular complexes in an ultrafast thulium fiber laser, Commun. Phys. **5**, 302 (2022).

[55] S. Huang, Y. Liu, H. Liu, Y. Sun, R. Xia, W. Ni, Y. Luo, L. Yan, H. Liu, Q. Sun, P. P. Shum, and X. Tang, Isomeric dynamics of multi-soliton molecules in passively mode-locked fiber lasers, APL Photonics **8**, 036105 (2023).

[56] A. Komarov, K. Komarov, and F. Sanchez, Quantization of binding energy of structural solitons in passive mode-locked fiber lasers, Phys. Rev. A **79**, 033807 (2009).